IOPscience iopscience.iop.org

Home Search Collections Journals About Contact us My IOPscience

Stress-enhanced pattern formation on surfaces during low energy ion bombardment

This article has been downloaded from IOPscience. Please scroll down to see the full text article.

2009 J. Phys.: Condens. Matter 21 224021

(http://iopscience.iop.org/0953-8984/21/22/224021)

View the table of contents for this issue, or go to the journal homepage for more

Download details:
IP Address: 129.252.86.83
The article was downloaded on 29/05/2010 at 20:02

Please note that terms and conditions apply.

IOP PUBLISHING JOURNAL OF PHYSICS: CONDENSED MATTER
J. Phys.: Condens. Matter **21** (2009) 224021 (7pp) doi:10.1088/0953-8984/21/22/224021

Stress-enhanced pattern formation on surfaces during low energy ion bombardment

N V Medhekar[1], W L Chan[2], V B Shenoy[1] and E Chason[1]

[1] Brown University, Division of Engineering, Providence, RI 02192, USA
[2] Department of Materials Science and Engineering, University of Illinois at Urbana-Champaign, Urbana, IL 61801, USA

E-mail: Nikhil_Medhekar@brown.edu, WLChan@uiuc.edu, Vivek_Shenoy@Brown.edu and Eric_Chason@Brown.edu

Received 28 January 2009
Published 12 May 2009
Online at stacks.iop.org/JPhysCM/21/224021

Abstract
Ion-induced surface patterns (sputter ripples) are observed to grow more rapidly than predicted by current models, suggesting that additional sources of roughening may be involved. Using a linear stability analysis, we consider the contribution of ion-induced stress in the near surface region to the formation rate of ripples. This leads to a simple model that combines the effects of stress-induced roughening with the curvature-dependent erosion model of Bradley and Harper. The enhanced growth rate observed on Cu surfaces appears to be consistent with the magnitude of stress measured from wafer curvature measurements.

(Some figures in this article are in colour only in the electronic version)

1. Introduction

It is well known that surface patterns can be spontaneously induced by low energy ion beam sputtering of amorphous and crystalline surfaces [1–4]. In many cases, the feature sizes of the observed patterns are in the nanometer scale, making them potentially suitable for sublithographic surface templating. A wide range of morphologies and growth kinetics have been observed under different conditions and a corresponding range of models have been proposed to explain the observations. Although these models explain many features that have been observed, current models cannot quantitatively predict the observed rate of pattern formation.

One of the most extensively studied forms of ion-induced patterning are sinusoidal modulations known as sputter ripples that have been described by a theory developed by Bradley and Harper (BH) [5]. BH showed that the formation of these patterns can be understood on the basis of a competition between the surface roughening caused by the ion beam [6] and the smoothening driven by surface diffusion. Extensions to the linear model have been proposed to include other mechanisms [2] and non-linear effects [1, 7]. These models have been successful at explaining qualitatively many features of ripple formation such as the orientation, exponential increase in amplitude, fixed wavelength and many others [3].

However, measurements on metal and semiconductor surfaces show that during early stages of ripple formation, the measured rates of growth of ripple amplitudes can be orders of magnitude larger than the predictions of the BH theory [3, 8–13]. These experiments therefore motivate us to consider additional roughening mechanisms that can potentially account for enhanced roughening rates observed on crystalline surfaces. In this work we consider the effect of ion-induced stress in the near surface region as an additional source of roughening that contributes to the ripple formation. We show that stress can significantly increase the growth rates of ripples above the predictions of the theoretical models. The source of this stress is the implantation of the energetic ion into the lattice as well as the subsequent creation of point defects such as vacancies, interstitials and their clusters. Depending on the formation, annihilation and recombination rates of the implanted ion and associated defects, a steady state stress on the order of 1–5 GPa can develop in the top surface layers [12, 14]. In the following, we describe a model that incorporates the roughening induced by stresses into the linear stability analysis of ripple formation and provide quantitative estimates for the enhancement in their growth rates. Comparison of our analysis with Cu measurements suggest that the stress effects are a significant contribution to

 © 2009 IOP Publishing Ltd Printed in the UK

the growth enhancement, although other effects such as non-linear terms [1], effects of kinetic barriers at the step edges [2] and mass redistribution [15] may play a role.

2. Background and theory

2.1. Stress-induced roughening

It has been noted in several works that stress in the surface can lead to pattern formation on surfaces. Asaro and Tiller [16] and Grinfeld [17] have pointed out how stressed surfaces are unstable with respect to surface undulations. Alternatively, strained layers can also undergo a transition to the formation of self-assembled arrays of clusters or quantum dots which has been observed extensively in semiconductor systems, e.g., SiGe on Si [18], InGaAs on GaAs [19] and many other systems. In either case, the driving force for the transition is the reduction in strain energy that can be induced by changes in the surface morphology. For different sputtering conditions and materials systems, both of these types of morphologies (sinusoidal ripples and quantum dots) have been observed [3, 20, 21] on sputtered surfaces.

In the following, we focus on the development of sinusoidal ripple morphologies due to stress in the surface layers. The kinetics of the pattern formation has been described in terms of a linear stability analysis by Srolovitz [22]. The stress in the layer leads to a change in the amplitude of the different Fourier components (h_k) with wavevector k on the surface:

$$\frac{\partial h_k}{\partial t} = (Ck^3 - Bk^4)h_k. \tag{1}$$

The k^3 term comes about from the reduction in elastic energy by the rippling of the surface. The parameter C is given by

$$C = \frac{D_s \Omega^2 \rho}{k_B T} \frac{(1-\nu^2)\,\sigma_m^2}{E}, \tag{2}$$

where D_s is the surface diffusivity, ρ is the concentration of mobile species on the surface and Ω is the atomic volume. E is the elastic modulus, ν is the Poisson ratio and σ_m is the stress in the surface layer.

The k^4 term arises from the decrease in ripple amplitude by the action of surface diffusion. Driven by chemical potential gradients, surface diffusion acts to decrease the surface energy by decreasing the amplitude of the surface height. This process has been shown by Mullins [23] and Herring [24] to depend on the divergence of the surface curvature. The parameter B is given by

$$B = \frac{D_s \Omega^2 \rho}{k_B T}\gamma, \tag{3}$$

where γ is the surface free energy.

Equation (1) has solutions of the form

$$h_k = h_k^0\, \mathrm{e}^{rt}, \tag{4}$$

where r is given by

$$r = Ck^3 - Bk^4. \tag{5}$$

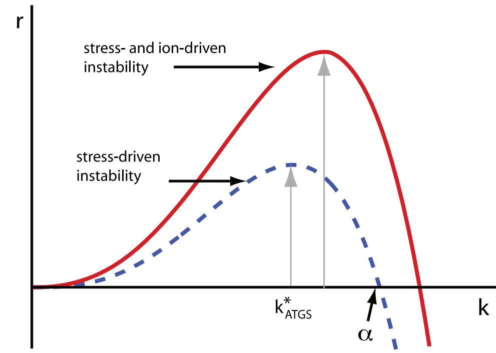

Figure 1. Schematic showing amplification rate r versus magnitude of wavevector for ripples induced by stress only and by combined stress and ion bombardment.

This equation describes the growth rate of surface features as a dynamic balance between roughening and smoothing induced by the competition between strain energy and surface energy. The wavelength dependence of the different kinetic processes determines which spatial frequencies will grow and which will decay.

The value of the amplification factor r as a function of wavevector is shown schematically in figure 1 by the curve labeled as 'stress-driven instability'. For small values of the spatial frequency k, the decrease in strain energy dominates. This makes the value of r positive so that the ripples with these spatial frequencies will grow with time. For large values of k, surface diffusion dominates and r is negative so that ripples with these spatial frequencies will decay with time. We define a critical value for the wavevector, α, as

$$\alpha \equiv \frac{C}{B} = \frac{(1-\nu^2)\,\sigma_m^2}{E} \tag{6}$$

which separates the band of unstable wavevectors ($k < \alpha$, $r > 0$) from the band of stable wavevectors ($k > \alpha$, $r < 0$).

The maximum growth rate occurs at the wavevector k^*_{ATGS} (referred to as ATGS for Asaro–Tiller–Grinfeld–Srolovitz) at the rate r^* given by

$$k^*_{\mathrm{ATGS}} = \tfrac{3}{4}\alpha; \tag{7a}$$

$$r^* = \tfrac{27}{256}\alpha^3 C = \tfrac{1}{4} C k^{*3}_{\mathrm{ATGS}} \tag{7b}$$

and is shown by the vertical arrow on the figure. The surface therefore develops a characteristic periodicity with this value as its wavevector. Note that the periodicity of the pattern depends only on the value of the stress and the elastic constants and is independent of the surface diffusivity. The growth rate, on the other hand, does depend on the diffusivity, as well as being a strong function of the stress in the layer ($\sim\sigma_m^8$).

2.2. Ion-induced roughening

The BH [5] theory of ion-induced ripple formation follows a similar formalism to the stress-induced roughening analysis. In the BH model, the roughening of the surface is induced by the ion-induced removal of atoms from the surface

(i.e., sputtering). The sputtering is based on a model developed by Sigmund [6] in which the incoming ion gives up its kinetic energy in a series of collisions. When averaged over many ion trajectories, the energy deposited into the near surface region is approximated by Gaussian ellipsoids around the nominal range of the ion. The rate of sputtering atoms from different sites on the surface is taken to be proportional to the amount of energy deposited at that site. BH and others [1, 5] calculated how this leads to a sputtering yield that is dependent on the surface curvature and the parameters describing the distribution of the energy deposited by the ion.

The BH model predicts that the amplitude of individual Fourier components evolves as:

$$\frac{\partial h_k}{\partial t} = (Ak^2 - Bk^4)h_k, \tag{8}$$

where

$$A = f\,a\,\Omega\,Y_0|\Gamma_{\max}| \tag{9}$$

f is the ion flux, a is the nominal range of the ion and Y_0 is the average sputter yield. Γ refers to the sputter roughening parameter; details can be found in [1] and [5]. The subscript max refers to the direction of the maximum roughening rate and hence the ripple orientation. x corresponds to the ripple wavevector aligned parallel to the direction of the incident ion projected onto the surface; y corresponds to the ripple wavevector aligned in the orthogonal direction on the surface.

The time dependence of each mode has the same form as equation (4). In this case, the preferred wavevector ($k^*_{\rm BH}$) and maximum growth rate (r^*) are given by

$$k^*_{\rm BH} = \sqrt{\frac{A}{2B}} \tag{10a}$$

$$r^* = \frac{A^2}{4B} = \frac{1}{2}A\,k^{*2}_{\rm BH}. \tag{10b}$$

Note that in the case of ion-induced roughening, the predicted wavevector does depend on the diffusivity, unlike the stress-induced roughening.

Since the BH model is based on a linear stability analysis, it is only expected to be applicable in the early stages of ripple formation. Non-linear terms have been proposed to explain the later stages of roughening, but the linear model is still expected to account for the initial dependence of the wavelength on the processing parameters [1, 25].

2.3. Combination of stress and ion roughening effects

As seen above, both stress- and ion-induced ripple formation can be understood in terms of a linear stability analysis and the rapid growth of a preferred unstable mode. In the following, we combine the two models together to study the simultaneous effects of sputtering and stress on surface evolution. In order to do this, we adopt the following simplifying assumptions: (1) the stress induced by the ion bombardment is assumed to be equi-biaxial and uniform in a region near the surface that is much larger than the amplitude of the ripples; and (2) the sputtered solid is assumed to be linear elastic with isotropic elastic properties.

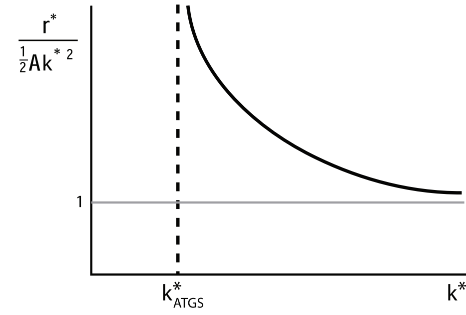

Figure 2. Variation in the normalized exponential rate of growth ($r^*/\frac{1}{2}Ak^{*2}$) with the fastest growing wavevector k^*.

With these assumptions, the surface morphology evolves due to the combined effects of roughening from sputter erosion and defect-generated stresses and surface relaxation due to capillary forces. The result has the same form as equation (4) with the growth rate given by:

$$r = Ak^2 + Ck^3 - Bk^4. \tag{11}$$

The corresponding preferred wavevector (k^*) and maximum growth rate (r^*) are

$$k^* = \tfrac{1}{2}k^*_{\rm ATGS} + \sqrt{\left(\tfrac{1}{2}k^*_{\rm ATGS}\right)^2 + {k^*_{\rm BH}}^2} \tag{12a}$$

$$r^* = \frac{1}{2}Ak^{*2} + \frac{1}{4}Ck^{*3} = \frac{1}{2}Ak^{*2}\left[1 + \frac{k^*_{\rm ATGS}}{3(k^* - k^*_{\rm ATGS})}\right]. \tag{12b}$$

Note that for the case of no stress ($C = 0$) or no ion bombardment ($A = 0$) the solutions revert to the same form as for the individual processes described above.

The variation of r for the combined action of stress and ion bombardment is shown schematically in figure 1 (labeled as 'stress-and ion-driven instability') for comparison with the case of stress alone. The combination of stress and sputtering is seen to increase the magnitude of k^*, i.e., the wavevector that grows the fastest, and also to increase the rate of growth for all unstable wavevectors.

Figure 2 qualitatively illustrates the enhancement of the ion-induced roughening rate by stress relative to the rate of growth predicted by the BH model alone ($\frac{1}{2}Ak^{*2}$). When $k^* \gg k^*_{\rm ATGS}$, the contribution of stress is negligible and the fastest mode grows at the rate predicted in the BH analysis. However, when k^* is close to $k^*_{\rm ATGS}$, the roughening of the ripples is dominated by the ion-induced stresses resulting in a larger growth rate than would be produced by sputtering alone.

3. Stress induced by low energy ions

Ion bombardment can induce stress in the near surface region due to processes such as implantation of the bombarding species and the subsequent production of defects (interstitials and vacancies) as shown schematically in figure 3. Volumetric expansion and relaxation around the implanted ion and other defects create stress in the layer. The evolution of the stress

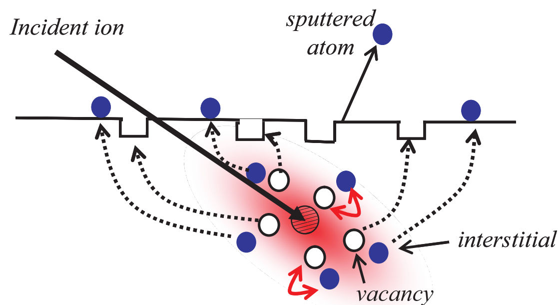

Figure 3. Schematic diagram illustrating some processes occurring during ion bombardment. The incident ion loses energy by collisions, generating vacancy and interstitial defects. The ion and defects can diffuse to the surface at different rates, annihilate by recombination or form clusters. Relaxation around each type of defects creates stress in the near surface region.

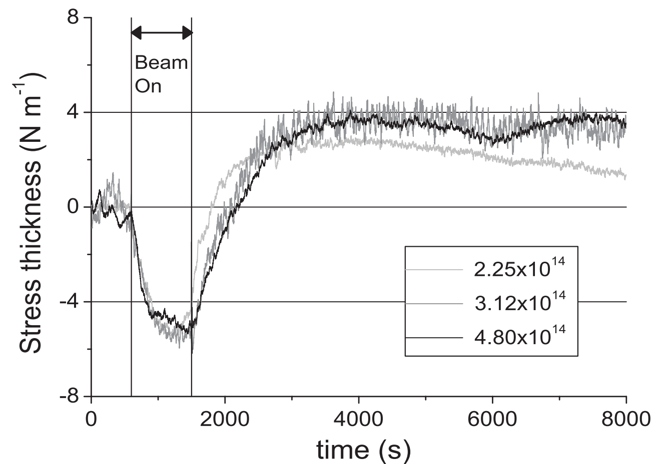

Figure 4. Measurement of the stress-thickness during low energy Ar ion sputtering of a Cu surface at different fluxes (2.25, 3.12 and 4.80×10^{14} cm^{-2} s^{-1}).

depends upon the number of defects produced and the kinetics controlling their subsequent evolution.

A number of previous studies have focused on the effects of high energy MeV ions [26–30], in which the stress evolution has been explained by ion-induced viscous flow [26, 29, 30] and plastic deformation induced by the ion [27–29]. At high energies, the implantation depth and relatively high stopping power are also sufficient to cause structural changes such as grain growth [31, 32]. At the low energy used in sputtering, the mechanisms for stress generation can be much different. Due to the shorter range and relatively low stopping power, the induced stress is more suitably described in terms of ion implantation and the point defects generated by the energetic ions.

Kalyanasundaram *et al* [33] calculated the stress induced in Si by sub-keV Ar ions using molecular dynamics (MD) simulation and found a compressive stress that reaches a steady state of 1.6 GPa for 700 eV Ar^+ ions. In comparison, measurements on Si(001) surfaces using wafer curvature techniques during ion bombardment find much lower values of the stress. In this technique, the measured curvature is proportional to the integral of the stress over the thickness of the stressed region (which is often referred to as the stress-thickness or the force per unit width). Conversion of the curvature to stress requires an estimate of the thickness of the stressed region, which is generally taken to be the range of the ion as estimated by SRIM [34]. Using this approach, Gozde *et al* [12] found a stress of ~0.08 GPa during 300 eV Ar^+ sputtering. Similarly, Zhao *et al* [35] measured stress in the range of 0.2–0.3 GPa, for 1–5 keV Ar^+ at fluxes of 10^{12} ion cm^{-2} s^{-1}.

The large discrepancy between the MD simulations and experiments may be due to the limited nanosecond time range of the simulation so that they neglect atomistic processes such as diffusion and recombination of defects which can have significant effects on the irradiation-induced stress. In addition, bombardment of semiconductors induces amorphization of the layer which enhances atomic transport and has a tendency to reduce stress and suppress ripple formation [8]. It has also been shown that seeding Si with a small amount of Mo atoms can result in significant enhancement in the surface stress [12].

Dahmen *et al* measured the surface stress induced on single crystal Cu by Ar ions as a function of energy, fluence and ion species [36] using a wafer curvature technique. The measurements found a compressive stress during bombardment that reached a steady state level of saturation. The steady state was explained in terms of a model that included compressive stress due to expansion of the lattice around the implanted Ar ion and the subsequent removal of these implanted ions by sputtering. Under this model, the defects are assumed to be immobile so the steady state stress depends on the depth of implantation (which depends on ion energy and species) but is independent of flux and temperature.

Chan *et al* [14] extended these studies by investigating the temperature and flux dependence of the stress generated during ion bombardment and the subsequent stress relaxation after the bombardment. The evolution of the stress during and after ion bombardment is shown in figure 4 where the period of ion bombardment is indicated by the region labeled 'beam on' in the figure. The large change in stress after the bombardment is terminated indicates that the defect concentration can evolve significantly and points to the importance of mobile defects in determining the steady state stress.

These measurements are explained in terms of a model in which ion-induced defects (implanted ions, vacancies and interstitials) are continuously created during bombardment. The stress in the layer is attributed to the different relaxation volumes around each type of defect; positive around interstitials and implanted ions and negative around vacancies. The concentration profile for the different defects is calculated numerically assuming that each type of defect has a different mobility which determines how rapidly it diffuses to the surface or recombines with others. The concentration of each defect reaches a different steady state value during sputtering, resulting in a steady state stress-thickness. The slow rate of diffusion of vacancies to the surface results in a residual tensile stress after the ion beam is terminated. Assuming an implantation depth for an Ar ion at this energy of 1–2 nm, they computed that the steady state during irradiation corresponds to an average stress in the surface region on the order of 1–2 GPa.

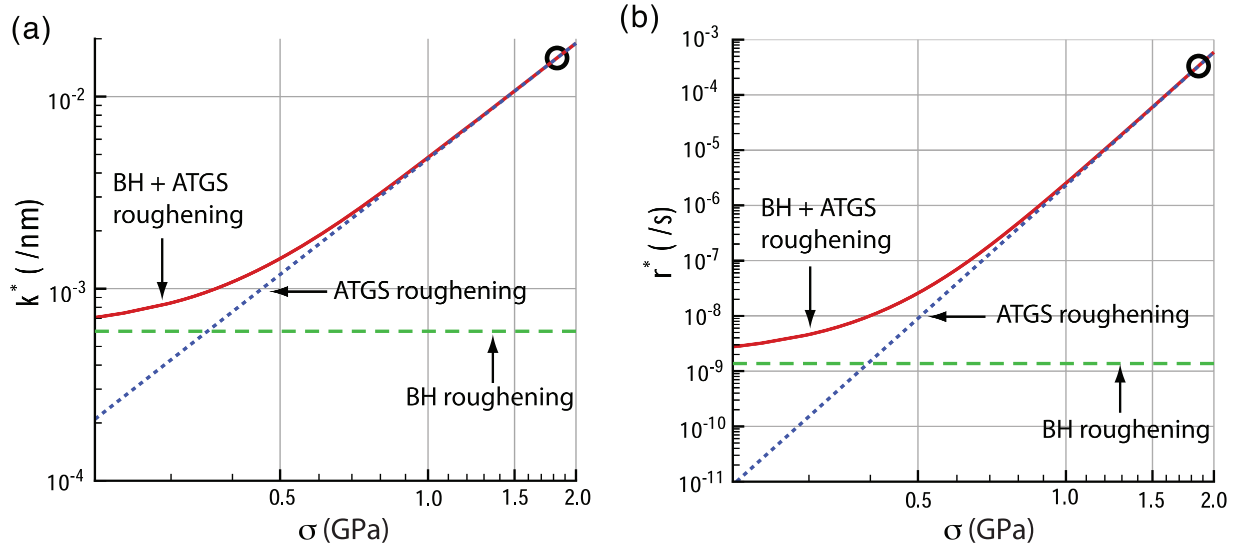

Figure 5. Stress dependence of (a) fastest growing wavevector k^* and (b) the rate of ripple growth r^*. The lines represent the variation of k^* and r^* with roughening due to the BH, ATGS and combined mechanisms. The parameters used for these plots correspond to the ripple growth on Cu(001) bombarded with Ar^+ ions. The encircled points represent the corresponding experimental measurements of k^* and r^*.

In the above discussion, it is assumed that the induced stress is uniform within the ion implantation range. However, recent measurements on nano-crystalline Pt films show that the stress profile can be much more complicated [37]. Because of the diffusion of ion-induced interstitials, compressive stress can be induced as far as 10 nm beyond the ion range. The stress determined by dividing the net change in stress-thickness by the thickness of the ion range may hence incorrectly estimate the near surface stress.

4. Relation of stress to ripple growth rate

To explore the validity of the linear model for stress-assisted sputter rippling, we compare the predictions with experimental results from sputtered Cu(001) surfaces. Estimates of the parameters were obtained from a combination of the BH theory and experimental studies. To estimate the parameter A, we used the BH model with parameters for the incident ion obtained from SRIM. The theoretically determined value of the roughening coefficient is $A = 4.6 \times 10^{-3}\ f\ \mathrm{nm}^2\ \mathrm{s}^{-1}$ in equations (9) where f is the magnitude of the flux in units of ions $\mathrm{nm}^{-2}\ \mathrm{s}^{-1}$. From measurements of the ripple growth kinetics on sputtered Cu(001) surfaces, we obtained r^* and k^* for sputtering with 800 eV Ar^+ ions at a flux $f = 2.1$ ions $\mathrm{nm}^{-2}\ \mathrm{s}^{-1}$. The resulting ripples form with wavelength of 396 nm ($k^* = 0.0158\ \mathrm{nm}^{-1}$) and grow exponentially with $r^* = 3 \times 10^{-4}\ \mathrm{s}^{-1}$ [10]. Note that the observed value of r^* is two orders of magnitude larger than that predicted by the BH model alone at this wavevector, i.e., $r^* = \frac{1}{2}Ak^{*2} = 1.24 \times 10^{-6}\ \mathrm{s}^{-1}$.

The observed values of k^* and r^* are used with A to determine the other parameters: $B = 136\,95\ \mathrm{nm}^4\ \mathrm{s}^{-1}$ and $C = 291.8\ \mathrm{nm}^3\ \mathrm{s}^{-1}$. The amount of stress in the surface can be estimated from these parameters using the definition of α in equation (6) and materials parameters $E = 120$ GPa, $\nu = 0.3$ and $\gamma = 1.2\ \mathrm{N\ m}^{-2}$ for Cu(001). The estimated value of the stress is 1.84 GPa, which is within the range estimated from wafer curvature measurements described above [14].

The predicted stress dependence of the wavevector k^* and the rate r^* for the ripple growth is shown in figure 5 as a function of the stress σ_m. The experimentally measured values are plotted on the figures as open circles; the value of stress associated with these measurements is obtained from the parameters B and C as described above. The calculated values of k^* and r^* as a function of stress (solid line) are obtained from the model using the values of the parameters described above and equations (7), (10), and (12). Note that the parameter C in the model is the only parameter that depends directly on the stress ($C \sim \sigma_m^2$). The stress dependence in figure 5 illustrates the cross-over from ion-induced roughening to stress-induced roughening as the magnitude of the surface stress increases. At low stress, the values of k^* and r^* asymptotically approach the BH theory (horizontal dashed line) which is independent of stress. As the stress increases, k^* and r^* start to follow the predictions of the ATGS theory, shown as the dotted line.

Depending on the stress in the surface layers and experimental conditions, we can identify two regimes of scaling for k^* and r^*. In the low-stress regime, $k^* \sim (f/D_s)^{1/2}$ and $r^* \sim f^2/D_s$. On the other hand, in the high-stress regime, the scaling laws are modified due to stress effects to $k^* \sim \sigma_m^2$ and $r^* \sim \sigma^8 D_s$. With these relations, one finds that for a small change of stress from 0.4 to 2 GPa, the rate of ripple growth r^* increases by five orders of magnitude while the wavevector k^* increases only by an order of magnitude.

The model can also be compared qualitatively with measurements on amorphized Si surfaces seeded with Mo where both stress and the patterning kinetics have been measured [12]. In these experiments, dot-like Si structures were observed rather than extended sinusoidal ripples, so the morphology is significantly different than the one for which our model was derived. Nevertheless, the amplitude of the

pattern was observed to grow exponentially with a preferred periodicity so it is possible to compare the measured growth rate with the prediction from the BH theory. The measured values obtained from the ripple formation are $r^* = 1.75 \times 10^{-3}$ s^{-1} and $k^* = 0.25$ nm^{-1}; this value of r^* is 40 times larger than the value predicted from the BH theory ($A = 1.4 \times 10^{-3}$ nm^2 s^{-1}). Using the calculated value of A, our model predicts that the observed enhancement in the growth rate can be obtained with a stress of $\sigma = 7.9$ GPa in the layer. This estimate is of the same order as the stress determined from wafer curvature measurements. Significantly, without the addition of the Mo seeds, the stress is significantly less ($\sim$0.08 GPa) and the surface remains smooth. This further points to the importance of stress in enhancing ion-induced pattern formation, even under different sputtering conditions.

5. Discussion

In this section, we discuss several factors related to the assumptions of our model and the generality of our results. In deriving the stress-enhanced ripple formation rate, we assumed that the stress is equi-biaxial so that it does not play a role in determining the orientation of the ripple pattern. The ripple orientation was taken to be determined by the maximum growth rate of the two modes predicted by the BH theory. However, the assumption of equi-biaxial stress may not be correct when the ion beam is incident in an off-normal direction and anisotropy in the ion-induced stress may influence the ripple direction. Studies are currently underway to measure the stress state during off-normal low energy sputtering to determine if this anisotropy is significant. In addition, the stress state may be more complex [37] than the uniform depth dependence assumed in the model. The wafer curvature techniques used to measure the stress can not directly determine the depth distribution of the stress and therefore may underestimate the stress contributing to the roughening.

The comparison of the Cu measurements with our model suggests that the observed rapid rate of ripple formation is much larger than expected from the BH theory so that it is driven mainly by stress effects. However, this analysis is based on comparing the measured value of r^* with the calculated rate based on the prediction of the BH theory. It is important to acknowledge that there may be limitations to the BH theory that underestimate the degree of roughening due to ion bombardment and therefore overestimate the effect of stress. In the first case, the calculated value of parameter A is based on the Sigmund theory of sputtering which likely underestimates the degree of roughening due to the curvature dependence of the sputter yield. Molecular dynamics simulations [15] of ion-impact craters suggest that significantly more mass rearrangement occurs during sputtering than predicted by the Sigmund theory which may increase the growth rate of ripples above the BH prediction even in the absence of any stress effects.

In addition, the BH theory considers only the surface morphology changes due to sputtered atoms and ignores the effects of the other ion-induced defects that may contribute to roughening. Other non-stress-related mechanisms may contribute to pattern formation; for instance, effects of Ehrlich–Schwoebel barriers to inter-level diffusion have been invoked to explain ripple growth on sputtered metal surfaces [2, 38]. Consequently, we caution that the apparent enhancement of the ripple formation rate in Cu should not be attributed solely to stress-related effects. The results described here should be taken to indicate that stress can play a significant role ion ion-induced pattern formation and its effect should be studied further.

In summary, we have shown that the relaxation of defect-generated stresses by surface undulations can be a significant additional driving force for ripple formation during sputtering of crystalline surfaces. Based on a simple linear stability analysis, we find there are two distinct regimes where the roughening is dominated either by curvature-dependent sputter yield or by the relaxation of defect-induced stresses. In the high-stress regime, we find that the rate of ripple growth is a strong function of stress in the surface layer, scaling as $r^* \sim \sigma^8$. Comparison with measurements of ion-induced stress and ripple formation suggest that stress-induced roughening plays a significant role in the rapid growth of ripples on Cu. Uncertainties in the sputtering parameters as well as the measured stress indicate the need for further studies to quantitatively determine the balance between ripple formation induced by sputter removal and by stress.

Acknowledgments

The research support of the US DOE under Contract No. DEFG02-01ER45913 is gratefully acknowledged as well as useful discussions with K Ludwig and M J Aziz.

References

[1] Makeev M A, Cuerno R and Barabasi A L 2002 *Nucl. Instrum. Methods Phys. Res.* B **197** 185
[2] Valbusa U, Borangno C and de Mongeot F R 2002 *J. Phys.: Condens. Matter* **14** 8153
[3] Chan W L and Chason E 2007 *J. Appl. Phys.* **101** 121301
[4] Munoz-Garcıa J, Vazquez L, Cuerno R, Sanchez-Garcıa J A, Castro M and Gago R 2009 Self-organized surface nanopatterning by ion beam sputtering *Lecture Notes on Nanoscale Science and Technology* ed Z Wang (Heidelberg: Springer)
[5] Bradley R M and Harper J M E 1988 *J. Vac. Sci. Technol.* A **6** 2390
[6] Sigmund P 1969 *Phys. Rev.* **184** 383
Sigmund P 1973 *J. Mater. Sci.* **8** 1545
[7] Cuerno R and Barabasi A L 1995 *Phys. Rev. Lett.* **74** 4746
[8] Chason E, Mayer T M, Kellerman B K, McIlroy D T and Howard A J 1994 *Phys. Rev. Lett.* **72** 3040
[9] Habenicht S 2001 *Phys. Rev.* B **63** 125419
[10] Chan W L, Pavenayotin N and Chason E 2004 *Phys. Rev.* B **69** 245413
[11] Brown A-D and Erlebacher J 2005 *Phys. Rev.* B **72** 075350
[12] Gozde O, Ludwig K F, Zhou H and Headrick R L 2008 *J. Vac. Sci. Technol.* B **26** 551
[13] Madi C S, Davidovitch B, George H B, Norris S A, Brenner M P and Aziz M J 2008 *Phys. Rev. Lett.* **101** 246102
[14] Chan W L and Chason E 2008 *J. Vac. Sci. Technol.* A **26** 44
[15] Kalyanasundaram N, Ghazisaedi M, Freund J B and Johnson H T 2008 *Appl. Phys. Lett.* **92** 131909

[16] Asaro R J and Tiller W A 1972 *Metall. Trans.* **3** 1789
[17] Grinfeld M A 1987 *Sov. Phys.—Dokl.* **31** 831
[18] Brunner K 2002 *Rep. Prog. Phys.* **65** 27
[19] Notzel R 1996 *Semicond. Sci. Technol.* **11** 1365
[20] Facsko S, Dekorsy T, Koerdt C, Trappe C, Kurz H, Vogt A and Hartnagel H L 1999 *Science* **285** 1551
[21] Frost F, Ziberi B, Hoche T and Rauschenbach B 2004 *Nucl. Instrum. Methods Phys. Res.* B **216** 9
[22] Srolovitz D J 1989 *Acta Metall.* **37** 621
[23] Mullins W W 1959 *J. Appl. Phys.* **30** 77
[24] Herring C 1950 *J. Appl. Phys.* **21** 301
[25] Kahng B, Jeong H and Barabasi A-L 2001 *Appl. Phys. Lett.* **78** 805
[26] Volkert C A 1991 *J. Appl. Phys.* **70** 3521
[27] Snokes E, Polman A and Volkert C A 1994 *Appl. Phys. Lett.* **65** 2487
[28] Trinkaus H and Ryazanov A I 1995 *Phys. Rev. Lett.* **74** 5072
[29] Snokes E, Weber T, Cacclato A and Polman A 1995 *J. Appl. Phys.* **78** 4723
[30] Brongersma M L, Snokes E and Polman A 1997 *Appl. Phys. Lett.* **71** 1628
[31] Misra A, Fayeulle S, Kung H, Mitchell T E and Nastasi M 1999 *Nucl. Instrum. Methods Phys. Res.* B **148** 211
[32] Mayr S G and Averback R S 2003 *Phys. Rev.* B **68** 214105
[33] Kalyanasundaram N, Moore M C, Freund J B and Johnson H T 2006 *Acta Metall.* **54** 483
[34] Ziegler J F and Biersack J P 1984–2000 *SRIM-2000.40* (Yorktown, NY: IBM Co.)
[35] Zhao K, Chan W L, Cahill D G and Averback R S 2008 private communication
[36] Dahmen K, Giesen M, Ikonomov J, Starbova K and Ibach H 2003 *Thin Solid Films* **428** 6
[37] Chan W L, Zhao K, Nhon V, Ashkenazy Y, Cahill D G and Averback R S 2008 *Phys. Rev.* B **77** 205405
[38] Cahill D G 2003 *J. Vac. Sci. Technol.* A **21** S110